SRC-TR-87-90

CHEMICAL PROCESS SYSTEMS LABORATORY

Evaporation of a Volatile Chemical From a Multicomponent Liquid Spill

by

Peter C. Cologer
Richard V. Calabrese

RESEARCH REPORT

CHEMICAL PROCESS SYSTEMS ENGINEERING LABORATORY

EVAPORATION OF A VOLATILE CHEMICAL FROM AMULTICOMPONENT LIQUID SPILL

Peter C. Cologer
Richard V. Calabrese

A CONSTITUENT LABORATORY OF
THE SYSTEMS RESEARCH CENTER

THE UNIVERSITY OF MARYLAND
COLLEGE PARK, MARYLAND 20742

Evaporation of a Volatile Chemical from a Multicomponent Liquid Spill

by

Peter C. Cologer** and Richard V. Calabrese*
Dept. of Chemical & Nuclear Engineering
University of Maryland
College Park, MD 20742

Submitted to
Chemical Engineering Science

* Address correspondence to R. V. Calabrese
** P. C. Cologer is presently with Dynatherm Corp., 1 Beaver Ct., Cockeysville, MD 21030

ABSTRACT

The evaporation of a volatile species from an otherwise non-volatile liquid spill is considered to assess the effects of initial composition and liquid phase resistance to mass transfer on evaporation rate. An idealized but reasonable general model is developed for the liquid phase. At the surface, vapor-liquid equilibria and mass transfer by wind convection are incorporated into a non-linear, third type, jump boundary condition. The resulting moving boundary value problem is solved numerically and the dimensionless surface flux and cumulative fraction evaporated are found to depend upon a modified Biot No., molecular weight ratio and initial mass fraction of volatile. Limiting case models are developed for the extremes of infinitely dilute versus pure fluid, and surface convection limited versus liquid phase diffusion limited behavior. Their range of applicability is determined by comparing their predictions with those of the general model. By estimating the range of Biot No. that might be encountered, it is shown that liquid phase resistance is important even for shallow spills and that detailed knowledge of vapor-liquid equilibria is often not required. Application of the models to real spills is discussed.

Introduction

The release of hazardous chemicals to the atmosphere due to accidental spillage of volatile liquids is a subject of great concern. Incidents involving road and rail tank cars can result in the vaporization of 5 to 75 m^3 of volatile liquid (Moein, 1978). Storage tank failures can lead to even larger releases. In the event of such accidents, those responsible for mitigation and public safety must know in what time frame they must act and require rational tools to estimate the potential consequences of the incident. These include fire and explosion hazard and exposure of response teams and the public to toxic vapors.

Numerous models exist to predict the rise and transport of gaseous substances on the winds, provided that the source term is known. For neutral density and buoyant plumes, validated plume rise models exist (e.g. Briggs, 1975). Many dispersion models can accomodate or can be adapted to include a time varying source of finite dimensions and chemical reaction with atmospheric constituents. Recently, much attention has been given to "heavier than air" emissions (e.g. Britter, 1979; Eidsvik, 1981; Fay and Ranck, 1983; de Nevers, 1984; Fay and Zemba, 1985). Calculation of evaporation rates (source term) for pure substances is relatively straightforward (Mackay and Matsugu, 1973) since there are no liquid phase concentration gradients and a lumped parameter approach, with time as the only independent variable, can accomodate most of the important physical phenomena. For the multicomponent case, liquid phase concentration gradients can result in a diffusional resistance to mass transfer which is not adequately accomodated by current

models. Furthermore, the importance of liquid phase diffusion has not been quantified.

Mackay and Matsugu (1973) modeled evaporation of gasoline by analogy to batch distillation. Calculated rates were higher than experimental measurements and the authors attributed this to use of the well mixed liquid phase assumption. Drivas (1982) developed an analytical lumped parameter (well mixed liquid) model for isothermal evaporation of hydrocarbon spills subject to the restriction that the ratio of surface area to total moles of liquid always remained constant. This implies that the spill shrinks in cross-section rather than in depth as evaporation proceeds. Feigley (1983) criticized his use of Raoults Law to describe the vapor-liquid equilibria, so Drivas provided a modified expression which accomodates constant liquid phase activity coefficients. The Drivas approach is based on modification of a model proposed by Harrison et. al. (1975) for evaporation of crude oil from sea-surface slicks. This model also accounted for losses to the immiscible water phase.

Some authors have considered the evaporation of small quantities of toxic substances from water pools of constant temperature and depth. Mackay and Yeun (1983) considered several organic solutes. In their experiments they maintained a well mixed liquid phase, via agitation, except for a thin surface boundary layer. They developed a correlation for the overall mass transfer coefficient which included both liquid and gas phase resistances. Bouwmeester and Vlek (1981a, 1981b) considered the release of ammonia from flooded rice fields and

ponded water. Their analytical model accounted for diffusional resistance in the liquid but assumed that the liquid depth was infinite and that the ammonia concentration was constant at the water-soil interface.

An exact model to predict the evaporation rate of a multicomponent spill should account for liquid and gas phase resistance, wind induced surface waves and convection cells, evaporative cooling and radiative heating. Furthermore, an evaporation proceeds the liquid depth decreases thereby slowing changes in the liquid phase composition. From a thermodynamic viewpoint, the liquid is seldom ideal. Concentration gradients can induce gradients in specific volume and mass diffusivity and the vapor and liquid compositions at the spill surface cannot be related simply. The resulting moving boundary value problem is quite complex and even if solvable, cannot be generalized to extract information on the relative importance of the various phenomena. The purpose of this work is to assess the effect of liquid phase diffusion and initial composition on evaporation rate. We therefore solve an idealized problem to determine when simpler models and thermodynamic relationships can be employed without subtantial loss of accuracy.

We consider the evaporation of a single volatile component from an otherwise non-volatile mixture. The liquid is assumed to be an ideal solution of constant temperature and mass diffusivity. Gas phase resistance and vapor-liquid equilibria are incorporated into a third type, moving boundary condition at the liquid-air interface. The partial differential equation which describes the spatial and temporal variation of liquid

phase composition is solved numerically and the time dependent surface vapor flux and cumulative fraction evaporated are thereby determined. The solution depends upon three parameters for which a sensitivity analysis is provided. Simpler models which apply to extremes in composition and predominant resistance to transfer are developed and their range of applicability is determined. Application of the models to real spills is discussed.

Theory

We refer to the volatile component as A and treat all non-volatile components as a single species B so that the spill can be treated as a binary mixture. It is assumed that spillage occurs instantaneously and the liquid is initially well mixed. The surface area is large compared to the initial uniform depth and remains constant as evaporation proceeds. There is no seepage into the ground. Then, the concentration of A is only a function of time and the vertical coordinate. At any time, t, the spill depth is L(t) with $L(0)=L_0$. The ground-liquid interface is at z=0 and the liquid-air interface (spill surface) is at z=L(t).

It is assumed that the background concentration of A in the atmosphere is negligible and that the liquid and vapor at the spill surface are in thermodynamic equilibrium. Dalton's Law applies. The molar flux of A at the spill surface or the evaporation rate per unit area is given by

$$N_A(z=L(t)) = K_m \bar{P}_A/RT \qquad (1)$$

where K_m is the gas side mass transfer coefficient and can therefore be estimated from correlations for evaporation of a

pure liquid. The partial pressure in the liquid is given by Raoult's Law or any convenient linear relationship so that Eq. 1 becomes

$$N_A(z=L(t)) = n_A(z=L(t))/M_A = K_m P_A^s X_A/RT \qquad (2)$$

Since Eq. 2 is a jump boundary condition for the liquid phase species continuity equation, it is tempting to employ a molar frame of reference (Toor, 1962). However, the total molar concentration is not constant since the molecular weights of A and B differ so it would remain as a variable in the resulting differential equation. Furthermore, this is not a case of equimolar counter diffusion so a molar average convection term would arise (Bird et. al., 1960). Most liquids are of similar density. For an ideal solution it is reasonable to assume that the total mass density remains constant thereby requiring equimass counter diffusion so that the process is purely Fickian in a mass frame of reference. The mass flux of A at time t in any vertical plane in the liquid is

$$n_A(z) = -\rho\, D_{AB} \frac{\partial w_A}{\partial z} \qquad (3)$$

The customary species continuity equation (Bird et. al., 1960) applies to a material coordinate system. Since mass is being lost from the liquid, an additional convection term arises which accounts for compression of the coordinate system and its effect on the concentration profile (Slattery, 1972). The liquid phase composition is therefore described by

$$\frac{\partial w_A}{\partial t} = D_{AB} \frac{\partial^2 w_A}{\partial z^2} - \frac{dL}{dt} \cdot \frac{\partial w_A}{\partial z} \qquad (4)$$

where dL/dt is the velocity of the surface given by

$$\frac{dL}{dt} = -\frac{1}{\rho} n_A(z = L(t)) \qquad (5)$$

The initial condition is $w_A=w_0$ at t=0. Since there is no seepage to the ground, the no flux boundary condition, $\partial w_A / \partial z = 0$, applies at z=0. The surface boundary condition follows from Eqs. 2 and 3 by converting mole fraction to mass fraction (Bird et. al., 1960).

$$n_A(z = L(t)) = -\rho D_{AB} \frac{\partial w_A}{\partial z} = \frac{K_m P_A^s M_B}{RT} \frac{w_A}{1 + (M_A/M_B - 1)w_A} \qquad (6)$$

The initial mass of A per unit area of spill is $\rho w_0 L_0$. The amount evaporated up to time t is obtained by integrating the surface flux so that the cumulative fraction of A evaporated is given by

$$f_A = \frac{1}{\rho w_0 L_0} \int_0^t n_A(z = L(t))dt \qquad (7)$$

It is appropriate to solve the equations in dimensionless form by defining dimensionless time $\tau = D_{AB}t/L_0^2$, distance $\eta = z/L_0$, spill depth $h=L/L_0$, concentration $w=w_A/w_0$, and mass flux $n'_A=n_A L_0/(w_0 \rho D_{AB})$. The dimensionless differential equation is

$$\frac{\partial w}{\partial \tau} = \frac{\partial^2 w}{\partial \eta^2} - \frac{dh}{d\tau}\cdot\frac{\partial w}{\partial \eta} \qquad (8)$$

$$\text{at } \tau = 0,\ w = 1 \qquad (9)$$

$$\text{at } \eta = 0,\ \frac{\partial w}{\partial \eta} = 0 \qquad (10)$$

$$\text{at } \eta = h(\tau),\ n_A'(\eta = h(\tau)) = -\frac{\partial w}{\partial \eta} = \frac{Bi\ w}{1 + w_0(\alpha-1)w} \qquad (11)$$

where $Bi=K_m L_0 P_A^s M_B/(D_{AB}\,\rho\,RT)$ is a modified Biot No. and $\alpha = M_B/M_A$ is the molecular weight ratio. The dimensionless surface velocity is

$$\frac{dh}{d\tau} = -w_0\ n_A'(\eta=h(\tau)) \qquad (12)$$

with h(0)=1. The fraction of A evaporated is

$$f_A = \int_0^\tau n_A'(\eta=h(\tau))\,d\tau \qquad (13)$$

When evaporation of A is complete, $f_A = 1$ and $h = w_0$.

It is seen that three parameters, Bi, w_0 and α, govern the solution. A more compact form is possible for certain limiting cases. The above will subsequently be referred to as the general model. A formal and detailed derivation is given by Cologer (1986).

Numerical Solution

The numerical solution to the general model utilizes a predictor-corrector process based on an implicit, forward difference scheme. Movement of the top boundary is accomodated by employing a variable number of spatial grid blocks and a variable top grid size (Crank, 1975). First derivatives are given as forward difference fractions and the spatial second derivative is a three point central difference fraction in the

forward time step (Carnahan et. al., 1969).

During the predictor phase of each time step, liquid level effects are ignored. The moving boundary convection term on the right hand side of Eq. 8 is deleted and the simplified equation is represented numerically by

$$-r\, w_{i+1,J+1} + (1+2r)\, w_{i,J+1} - r\, w_{i-1,J+1} = w_{iJ} \qquad (14)$$

for the bulk liquid. Subscripts i and J refer to spatial and temporal points, respectively and $r = \Delta\eta/\Delta\tau^2$. Near the boundaries, the finite difference equations incorporate the boundary conditions, uneven grid spacing at the top (liquid-air surface), and an imaginary grid point one step beyond both the top and bottom (Davis, 1984). The bottom, no flux boundary condition of Eq.10 is given by

$$(w_{1,J+1} - w_{-1,J+1})/2\,\Delta\eta = 0 \qquad (15)$$

The top, jump boundary condition of Eq. 11 is given by

$$\frac{(w_{m+1,J+1} - w_{m-1,J+1})}{2\,P\,\Delta\eta} + \frac{Bi\; w_{m,J+1}}{1 + w_0(\alpha-1)\; w_{m,J}} = 0 \qquad (16)$$

where P defines the relative size of the top grid block and i = m is the grid point at the evaporating liquid surface. The mass fraction in the denominator of the second term is equal to its present value. This contributes an explicit character to the numerical scheme thereby increasing its sensitivity to the size of the time step. However, use of a more cumbersome nonlinear representation of the top boundary is avoided. Therefore the matrix of unknown coefficients remains tridiagonal and is readily inverted.

At the end of the predictor phase, summation of the normalized mass fractions at each grid point, weighted by the size of the two neighboring grid blocks, gives the dimensionless mass of A remaining in the spill. The present surface flux is most accurately determined by subtracting this mass from that at the end of the previous time step and dividing by $\Delta\tau$. The present f_A follows from summation of the mass evaporated over all previous time steps. The value of P, and after several time steps that of m, is directly updated since, for a constant density system, the mass remaining and the spill depth are directly related.

Dropping the liquid level displaces the top layer of A and B whose mass must be incorporated into the liquid remaining below. During the corrector phase, the weight fraction profile resulting from the predictor phase is modified according to the moving boundary convection term of Eq. 8 by maintaining conservation of mass of both species. This corrected profile is used as the starting point for the predictor phase of the next numerical time step.

A sensitivity analysis of solution stability dictated the use of 100 spatial grid blocks and a time step size $\Delta\tau = \Delta\eta^2/2Bi$ for $\alpha \leq 10$. The time for complete evaporation increases with α. For $\alpha > 10$, $\Delta\tau$ was increased to keep the total number of time steps approximately equal. The details of the numerical procedure and the computer code are given by Cologer (1986). The scheme is readily adapted to nonideal vapor-liquid equilibria by treating P_A^s in Bi as a pseudo vapor

pressure and updating Bi at each time step.

Limiting Case Models

Several limiting case models have been developed to validate the numerical scheme of the general model and to determine the conditions for which simpler, more easily applied models are adequate. In general, the evaporation rate depends upon Bi, w_0 and α. In a coordinate system in these variables, regions will exist in which a limiting case model will give the same results as the general model. The extent of these regions can be determined by comparison.

For the limiting case models, the assumptions of the general case apply but additional simplifications are possible. One type of limiting behavior depends upon the predominant resistance to mass transfer. This is primarily determined by the Biot No. which is the ratio of the transfer rate at the surface by wind convection to that to the surface by diffusion. For small Bi, the major resistance is in the gas. Liquid phase diffusion is rapid so concentration gradients are small and the well mixed assumption applies. This is referred to as the convection limited case. For large Bi, the major resistance is in the liquid. Concentration gradients are steep and the surface liquid is rapidly depleted in A. This is termed the diffusion limited case. The critical values of Bi which determine these behavioral extremes depend upon w_0 and α. A second type of limiting behavior is based upon initial mixture composition and corresponds to evaporation of trace quantities of A and evaporation of pure A. The former is referred to as the infinite dilution case and the latter as the pure liquid case.

It is useful to understand the significance of extremes in α. For $\alpha \to 0$, $M_A >> M_B$ so that the mole fraction of A is small compared to w_0 and the spill is infinitely dilute in A on a molar basis. $\alpha \to \infty$ corresponds to almost pure A on a molar basis.

Convection Limited Model. For a well mixed spill, the surface flux is given by the right hand side of Eq.6 and w_A is only a function of time. A species material balance yields

$$-\rho \frac{d}{dt}(Lw_A) = n_A(z=L(t)) = \frac{K_m P_A^s M_B}{RT} \frac{w_A}{1 + (M_A/M_B - 1) w_A} \quad (17)$$

at t=0, $w_A=w_0$ and $L=L_0$

Although D_{AB} does not enter, it is convenient, for comparison purposes, to recast Eq. 17 in terms of previously defined dimensionless variables.

$$-\frac{d}{d\tau}(hw) = n_A'(\eta=h(\tau)) = \frac{Bi\ w}{1 + w_0(\alpha-1)w} \quad (18)$$

at $\tau = 0$, w=1 and h=1

Eq. 13 still applies and the quantities of interest still depend upon all 3 parameters. However, use of $\tau_c = Bi\ \tau$ and $n_A^c = n_A'/Bi$ results in a solution which depends only upon w_0 and α.

Since we must solve simultaneously for w and the spill depth, a second relationship is required. It is inherent in the following explicit numerical scheme. At the beginning of each time step, w, f_A and the spill depth are known from the previous time step. This w is used to calculate the current surface flux from the right hand side of Eq. 18. The mass of A evaporated is computed, used to update f_A and removed from the

liquid. The spill depth and composition are updated via a simple mass balance. The procedure is repeated until all A has evaporated.

In practice, the convection limited model is more conveniently applied using molar quantities and Eq. 1 or 2. Furthermore, it is readily adapted to non-ideal mixtures by updating the partial pressure and specific volume at each time step.

Diffusion Limited Model. At large Bi, liquid A diffusing to the surface is rapidly swept away. Except for small t, the surface w will be close to zero. Eq. 11 can therefore be replaced by a zero concentration boundary condition. The general numerical scheme can be modified accordingly and an explicit treatment of the surface boundary condition is no longer necessary. Quantities of interest will no longer depend upon Bi or α.

Infinite Dilution Models. Three infinite dilution models were developed. These are a two resistance model which applies to all Bi, a convection limited model which only applies at low Bi, and a diffusion limited model which only applies at high Bi.

If w_0 is small the liquid depth remains constant as evaporation proceeds. Thus $dh/d\tau = 0$, $h(\tau) = 1$ and $w_0 (\alpha-1)w \ll 1$ provided that α is not too large. This insures that the initial mole fraction of A is also small and that the mean molecular weight is equal to M_B. With these simplifications, Eqs. 8 to 11 reduce to

$$\frac{\partial w}{\partial \tau} = \frac{\partial^2 w}{\partial \eta^2} \qquad \text{at } \tau=0,\ w=1$$

$$\text{at } \eta=0,\ \frac{\partial w}{\partial \eta} = 0 \qquad \text{at } \eta=1,\ \frac{\partial w}{\partial \eta} + Bi\ w = 0 \tag{19}$$

Eq. 19 can be solved analytically to yield

$$w = 2 \sum_{n=0}^{\infty} e^{-\lambda_n^2 \tau} \frac{Bi}{\lambda_n^2 + Bi^2 + Bi} \frac{\cos \lambda_n \eta}{\cos \lambda_n} \tag{20}$$

where the eigenvalues are the roots of $\lambda_n \tan \lambda_n = Bi$. The evaporation rate is found by substituting Eq. 20 into the dimensionless form of Eq. 3 and evaluating the result at $\eta = 1$.

$$n_A'(\eta=1) = 2 \sum_{n=1}^{\infty} e^{-\lambda_n^2 \tau} \frac{Bi^2}{(\lambda_n^2 + Bi^2 + Bi)} \tag{21}$$

The cumulative fraction of A evaporated up to time τ is found by substituting Eq. 21 into 13 and integrating to obtain

$$f_A = 2 \sum_{n=0}^{\infty} (1-e^{-\lambda_n^2 \tau}) \frac{Bi^2}{\lambda_n^2(\lambda_n^2 + Bi^2 + Bi)} \tag{22}$$

We will refer to Eqs. 20 to 22 as the two resistance infinite dilution model.

More limited infinite dilution models can be developed by considering the magnitude of Bi. A convection limited, infinite dilution model is obtained from Eq. 18 by noting that now $h(\tau) = 1$ and $w_0 (\alpha - 1)w << 1$. Analytical integration and subsequent manipulation yield

$$w = e^{-Bi\ \tau} \tag{23}$$

$$n_A'(\eta = 1) = Bi\ e^{-Bi\ \tau} \tag{24}$$

$$f_A = 1 - e^{-Bi\ \tau} \tag{25}$$

A diffusion limited, infinite dilution model is obtained by

replacing the surface boundary condition of Eq. 19 by w = 0 at $\eta = 1$. The results are

$$w = 2 \sum_{n=0}^{\infty} e^{-(n + 1/2)^2 \pi^2 \tau} \frac{(-1)^n}{(n + 1/2)\pi} \cos(n + 1/2)\pi\eta \quad (26)$$

$$n_A'(\eta=1) = 2 \sum_{n=0}^{\infty} e^{-(n + 1/2)^2 \pi^2 \tau} \quad (27)$$

$$f_A = 2 \sum_{n=0}^{\infty} \frac{(1-e^{-(n + 1/2)^2 \pi^2 \tau})}{(n + 1/2)^2 \pi^2} \quad (28)$$

For the two resistance and convection limited infinite dilution cases, quantities of interest depend only on Bi. For the diffusion limited case they are also independent of Bi. As before, the Bi dependency can be absorbed for the convection limited case by use of τ_c and n_A^c.

These models can be applied to a broader class of mixtures than those for finite w_0 by replacing P_A^s in the definition of Bi with a Henry's Law constant.

Pure Liquid Evaporation Model. The evaporation of pure A is given by Eq.2 with $X_A = 1$. Since the surface flux is constant, $f_A = n_A(z=L(t))t/(\rho L_0)$. Although D_{AB} and M_B are not relevant, previously defined dimensionless variables are used for comparison with the general model. Then

$$n_A'(\eta=1) = \bar{n}_A(\eta=1) = Bi/\alpha \quad (29)$$

$$f_A = Bi\ \tau/\alpha \quad (30)$$

where $\bar{n}_A = w_0 n_A'$. Evaporation is complete when $f_A = 1$ or $\tau = \alpha/Bi$.

Results

The general model was applied to various combinations of Bi,

w_0 and α. Systematic trials were performed for the range $10^{-1} \leq Bi \leq 10^5$; $0.01 \leq w_0 \leq 0.99$; and $1 \leq \alpha \leq 1{,}000$. Other combinations were employed as necessary. The region $\alpha < 1$ was not considered since the volatile species is usually of lower molecular weight. The limiting case models were used to scope and verify the general model. Typical results are given below. A larger sample is given by Cologer (1986).

Liquid phase concentration profiles for $w_0 = 0.5$ and $\alpha = 1$ are given in Figure 1. At Bi = 0.1 the profiles are flat indicating that the spill is well mixed and mass transfer is convection limited. As Bi increases gradients become progressively steeper and the surface concentration, w_s, decreases relative to the bulk or average concentration within the spill. Eventually, w_s approaches zero indicating that transfer is diffusion limited. Similar trends occur for other w_0 and α but at higher transitional values of Bi.

The effect of initial composition on the fraction of A evaporated is given for $\alpha = 1$ in Figure 2. The curves labeled A and E result from the two resistance infinite dilution and pure fluid models, respectively. At constant Bi the curves for constant w_0 lie in order in an envelope between the infinite dilution and pure fluid limits. The evaporation time decreases as w_0 increases even though more A is initially present. For $\alpha = 1$, mole and mass fractions are equal and Eq. 11 reduces to $n_A' = Bi\ w$. Therefore w is a measure of the surface partial pressure relative to the vapor pressure contained within Bi. With decreasing w_0, the decrease in $\bar{P}_A$ is greater than that in the

amount to be evaporated. This type of behavior will be referred to as that determined by partial pressure.

Since the surface concentration decreases relative to the bulk as Bi increases, the $w_0 = 0.9$ curves of Figure 2 increasingly deviate from the pure fluid curves. This effect becomes less pronounced as w_0 decreases so the envelope of curves broadens. Despite the drop in relative surface concentration, the evaporation time decreases as Bi increases. Therefore, enhanced mass transfer due to increased Bi more than compensates for the decrease in relative partial pressure.

Certain conclusions at $\alpha = 1$ do not apply to higher α since the ratio of mole to mass fraction increases with α. For $w_0(\alpha-1)\, w >> 1$, Eq.11 reduces to $n_A' = Bi/w_0\, \alpha$ or $\bar{n}_A = Bi/\alpha$. The evaporation rate is equal to that for a pure liquid until large times when w_s becomes small. The evaporation time is primarily determined by the quantity of A initially present so it should increase with w_0. The curves of constant w_0 will lie in order to the right of the infinite dilution curve so the behavior is opposite that determined by partial pressure. The C and D series curves of Figure 3a display quantity determined behavior. The envelope broadens and the evaporation time increases with α since the amount of A on a molar basis increases. The infinite dilution curve applies to all α and the effect of α on evaporation time decreases as $w_0 \to 0$, as it should.

As α and w_0 decrease, actual behavior increasingly deviates from that for a pure fluid. A transition occurs from quantity to partial pressure determined behavior. The curves move to the left through the infinite dilution curve and their order must

reverse as $\alpha \to 1$. The B series curves of Figure 3a lie within this transition region. Curves for $\alpha = 100$ and $w_0 < 0.1$ would also be in transition. The behavior is complex and not easily qualified due to the competitive processes involved.

Figure 3a applies to Bi = 10 where w_s is relatively large so that quantity determined evaporation occurs for $\alpha \geq 100$ even at $w_0 = 0.1$. As Bi increases the relative surface concentration decreases so that $w_0(\alpha - 1)w$ in Eq. 11 may no longer be large even at high α and w_0. Pure fluid type evaporation diminishes and the effect of reduced partial pressure becomes more pronounced. Therefore a transition from quantity to partial pressure determined behavior is also caused by increased Bi. This is demonstrated at Bi = 1000 in Figure 3b where the curves for $\alpha = 100$ display partial pressure determined behavior and those for $\alpha = 1000$ have intersected the infinite dilution curve. The $\alpha = 1000$ curves will begin the reversal process at slightly higher Bi.

The B series curves of Figure 3b apply to $\alpha = 1$ and 10 indicating that the spill is diffusion limited for $\alpha \leq 10$ and for all w_0. For $\alpha = 100$ the spill is only diffusion limited for $w_0 \leq 0.1$. A comparison of Figures 3a and 3b shows that the evaporation time decreases as Bi increases for the same reasons as for the $\alpha = 1$ case. This decrease with Bi continues until a diffusion limited situation is encountered.

Figure 2 shows that at $\alpha = 1$, the infinite dilution assumption is valid for about $w_0 < 0.05$ and becomes slightly better as Bi increases due to a relative decrease in w_s. Figure 3 reveals that as α increases the $w_0 = 0.1$ and infinite dilution

curves increasingly deviate due to increased ratio of mole to mass fraction. For $\alpha = 1$ and $w_0 = 0.01$ the general and two resistance infinite dilution models always gave the same result. For $\alpha = 1000$ it was necessary to employ $w_0 < 10^{-4}$ to achieve congruence. The initial mole fraction appears to be the better criterion for invoking the infinite dilution assumption which should only be applied for $X_A < 0.05$.

A comparison of the $w_0 = 0.9$ and pure fluid curves of Figures 2 and 3 indicates that the pure fluid approximation improves as α increases due to increased ratio of mole to mass fraction. However, it deteriorates rapidly as Bi increases due to lower relative surface concentration. Congruence of the pure liquid and general model with $w_0 = 0.99$ hardly ever occurred except at low Bi and high α. Under these circumstances a convection limited (well mixed liquid) model is probably a better choice.

The transition from convection to diffusion limited behavior is conveniently seen by examining f_A as a function of Bi at constant w_0 and α. Figure 4 presents results at $w_0 = 0.3$. The A curve is predicted by the diffusion limited model and therefore applies to all appropriate Bi and α. The B and C series curves were determined from the general and convection limited models, respectively. Figure 4a reveals that at $\alpha = 1$, the spill becomes diffusion limited and the general model yields curve A for Bi slightly greater than 100 and larger. At Bi = 0.1 the convection limited and general model curves are congruent. At higher Bi the well mixed model underpredicts the evaporation time since it does not account for decreased surface partial pressure due to liquid

phase resistance to transfer.

Figure 4b presents similar results for $\alpha = 100$. As α increases so do the critical values of Bi which determine the onset of both limiting cases. This occurs since concentration gradients are not as large on a molar basis. Figure 5 is a similar plot developed using the three infinite dilution models and therefore applies to all α. The effect of w_0 on the transitional values of Bi is similar to that of α but for a different reason. As w_0 increases, longer evaporation times are required before there is considerable reduction in surface concentration.

By comparing the results of the general and limiting case models in terms of liquid phase concentration profile, surface flux and cumulative fraction of A evaporated, a regime plot was developed which allows determination of when the limiting case models are applicable. It is given in Figure 6. For a given α, the convection limited model is applicable below the lower or solid curve. The diffusion limited model can be applied above the upper or dashed curve. In between, the general model is recommended. The curves end slightly to the left of $w_0 = 1$ since evaporation of a pure liquid is always convection limited. However, the curves show the drastic effect that even small quantities of non-volatile component can have on spill behavior.

Although the limiting case models still require numerical computation except at infinite dilution, their solutions can be conveniently plotted. Figure 7 provides the diffusion limited solution which is independent of both Bi and α. In this regime

the evaporation time always decreases with increasing w_0 and the evaporation rate is determined by partial pressure since $w_s \rightarrow 0$. The convection limited solution, which is independent of Bi in terms of $\tau_c = Bi\ \tau$, is given in Figure 8. The evaporation time is determined by partial pressure at $\alpha = 1$ and by quantity at large α. For $1 < \alpha < 10$ the behavior is complex since the order of the curves must reverse. Fortunately, the numerical scheme is easily implemented.

While the cumulative fraction evaporated gives the time frame for emergency response and mitigation, plots of n_A' versus τ provide the source term for atmospheric dispersion models. Typical surface fluxes at $\alpha = 10$ are given in Figure 9. The curves provide additional insight into spill behavior. When comparing curves of constant w_0, recall that the definition of n_A' contains w_0 in its denominator. At Bi = 1000 the spill is diffusion limited so the curves A_1, B_1 and C_1 apply to all appropriate Bi and α (Figure 6). The flux decreases steadily as evaporation proceeds. At short times n_A' increases with w_0 due to increased surface partial pressure. At long times the reverse trend occurs since the evaporation time decreases as w_0 increases (Figure 7).

Like the evaporation time, n_A' decreases as Bi decreases. At shorter times n_A' becomes more constant and the order of the curves of constant w_0 reverse as the spill moves from partial pressure toward quantity determined behavior. Recall that for $\alpha \geq 10$, the surface flux approaches that of a pure liquid as Bi decreases (see Figure 3 discussion). The region of constant n_A' becomes broader with decreasing Bi and increasing W_0. The order

of the curves can reverse themselves several times. At Bi = 100, n_A' is initially smaller than at higher Bi. As evaporation proceeds, the surface becomes increasingly depleted in A and the curves collapse into those for a diffusion limited condition. At low Bi a convection limited condition is approached. The evaporation rate remains constant until long times and then falls rapidly since the spill has become significantly depleted. The order of the curves reverse since the evaporation time increases as w_0 increases (Figure 8). For $Bi \leq 1$ and $0.3 \leq w_0 \leq 0.5$, use of $n_A^c = n_A'/Bi$ in place of n_A' would result in curves that are independent of Bi; that is, n_A' increases directly with Bi. For all Bi, the effect of Bi on n_A' is greater than that of w_0.

Discussion

Application of the results to real spills requires an estimate of the range of Bi that can occur. The gas side mass transfer coefficient can be predicted from the correlation developed by Mackay and Matsugu (1973) for pure liquids.

$$K_m = 0.0292\ u^{0.78}\ d^{-0.11}\ Sc^{-0.67} \qquad (31)$$

where K_m = m/hr, u is the windspeed, m/hr, d is the effective spill diameter, m, and Sc is the Schmidt No. for species A in air. Eq. 31 was developed from wind tunnel data for the evaporation of cumene into a simulated atmospheric boundary layer. The correlation of Mackay and Yeun (1983) is less appropriate since it applies to the evaporation of slightly soluble organics from water bodies and includes liquid phase resistance due to a thin surface boundary layer above an

otherwise well mixed liquid.

The expected range of variables in Eq. 34 is $1 < u < 10$ m/s, $3 < d < 35$ m and $0.6 < Sc < 3.0$ for which $0.0016 < K_m < 0.036$ m/s. Typical molecular weights and vapor pressures for volatile species are $15 < M_A < 100$ and $0.2 < P_A^s < 2$ atm. Let $\rho = 1000$ Kg/m^3 and $T = 293^0$K. Consider the case $\alpha = 1$. Since the mixture is relatively inviscid, a reasonable range of liquid diffusivity is $0.5 \times 10^{-9} < D_{AB} < 2 \times 10^{-9}$ m^2/s. Then, for a spill of $L_0 = 1$ cm depth, $1 < Bi < 6400$. For an average condition, $Bi \approx 270$. For all w_0, Figure 6 shows that even these very shallow spills are never convection limited. Diffusion limited behavior is approached even for the average condition and the upper end of the Bi range extends well into this regime. Spills from diked tanks can be one to two orders of magnitude greater in depth pushing them farther toward diffusion limited behavior.

Most volatile species are of low molecular weight. Therefore, an increase in α is somewhat equivalent to one in M_B and the Bi range scales almost directly with α. For instance, at $\alpha = 100$ and $L_0 = 1$ cm, $100 < Bi < 64{,}000$. However, as M_B increases so does viscosity, so D_{AB} may decrease resulting in higher Bi. With this type of scaling Figure 6 reveals that the conclusions for $\alpha = 1$ apply at all higher .

It appears that liquid phase resistance to transfer is always signficant at least for the case of a single volatile component. The general model or its diffusion limited solution (Figure 7) is required except at infinite dilution where Eqs. 20 to 22 or 26 to 28 apply. This conclusion has some important practical consequences. In the presence of non-volatiles, a species A will

evaporate more slowly than would be predicted by a well-mixed liquid/lumped parameter model. For most spills the surface is substantially depleted in A within a short time after evaporation begins. Therefore it is not necessary to have detailed knowledge of the vapor-liquid equilibria. It is often sufficient to replace P_A^s in Bi by a Henry's Law constant or some pseudo vapor pressure applicable at low X_A. That is, the models can be reasonably applied even when the vapor liquid equilibira are non-ideal. Since evaporation is slow, evaporative cooling effects are not so important except at high heats of evaporation/ dissolution. The isothermal assumption is not as restrictive as first thought. The effect of cooling is to slow the evaporation rate so the models will still yield a conservative upper estimate.

On the other hand, the low surface partial pressure of the volatile component presents a seriouis limitation particularly for diffusion limited behavior. It may no longer be reasonable to assume that the components represented here as B are non-volatile. While the vapor pressure of B may be much less than that of A, its surface partial pressure can be a significant fraction of that of A. Evaporation of B will cause the spill depth to decrease more rapidly thereby concentrating the remaining A and increasing its evaporation rate. This may be somewhat counteracted by evaporative cooling so model estimates may still be reasonable.

Most spills will interact with soil or other ground surfaces. Despite the no flux boundary condition, the models can

be applied to the remaining liquid if seepage behavior can be quantified. The effective liquid pool will initially contain a concentration gradient but this should have little effect on the steep surface gradients which form rapidly and control the evaporation rate.

The assumption of constant mass density is not valid when component specific volumes are substantially different or when molecular interactions are strong. If ρ decreases as A evaporates the liquid level will not fall as rapidly. The spill will remain stable since the negative concentration gradients will cause negative density gradients. Actual concentration gradients will be smaller than predicted so the models will provide a conservative upper estimate of evaporation rates. If ρ increases, the liquid depth will drop more rapidly and positive density gradients may cause the spill to become unstable. While buoyant convection currents may cause the bulk of the liquid to tend towards well mixed, a liquid surface boundary layer of considerable resistance will still remain. Mass transfer will be enhanced and the process cannot be accurately simulated by the models presented here. A similar situation will occur at high wind speed due to wind driven surface waves and convection currents.

Since liquid phase resistance is significant when non-volatiles are present, it is reasonable to assume that it also plays an important role when all components are volatile. Relative to a well mixed liquid, the more volatile components will exhibit lower surface partial pressure and vice versa. A well mixed model will overpredict evaporation rates for the more

volatile species and underpredict those for the less volatile species.

Summary

For evaporation of a volatile species from an otherwise non-volatile multicomponent liquid spill, liquid phase resistance to mass transfer is significant. Lumped parameter (well mixed liquid) models will therefore overestimate the evaporation rate even for very shallow pools. A somewhat idealized numerical model has been developed which should yield reasonable estimates of evaporation rate except at high wind speed and heat of evaporation/dissolution, and for extremely non-ideal thermodynamic behavior. A regime plot has been developed (Figure 6) which allows one to determine when a simpler convection limited or diffusion limited model can be employed without substantial loss of accuracy. Analytical infinite dilution models can be employed for $X_A < 0.05$. Since most real spills approach diffusion limited behavior, the surface concentration of the volatile species is small. In many cases a Henrys Law constant can be used in place of detailed vapor-liquid equilibrium data to estimate the evaporation rate.

Acknowledgments

Computer facilities were provided free of charge by the University of Maryland Computer Science Center.

Nomenclature

Bi = $K_m L_0 P_A^s M_B/(D_{AB} \rho RT)$, modified Biot No.

D_{AB} = liquid phase mass diffusivity, m^2/s

d = effective spill diameter, m

f_A = cumulative mass fraction of A evaporated

h = L/L_0, dimensionless spill depth

K_m = gas side mass transfer coefficient, m/s

L = instantaneous spill depth, m

L_0 = initial spill depth, m

M_A = molecular weight of volatile species A

M_B = molecular weight of non-volatile species B

N_A = molar flux of A, $Kg/m^2 \cdot s$

n_A = mass flux of A, $Kg/m^2 \cdot s$

n_A' = $n_A L_0/(w_0 \rho D_{AB})$, dimensionless mass flux

$\bar{n}_A$ = $w_0 n_A'$, dimensionless mass flux

n_A^c = n_A'/Bi, dimensionless mass flux

$\bar{P}_A$ = partial pressure of A at liquid-air interface, atm

P_A^s = vapor pressure of A, atm

R = 82.05×10^{-6} $m^3 \cdot atm/g\ mole \cdot {}^0K$, universal gas constant

Sc = gas phase Schmidt No. for species A in air

T = absolute ambient temperature, ^0K

t = time, s

u = wind speed, m/s

w = w_A/w_0, normalized mass fraction of A

w_A = mass fraction of A in liquid

w_0 = initial mass fraction of A in liquid

w_s = normalized mass fraction of A at spill surface

X_A = mole fraction of A in liquid

z = vertical coordinate, m

Greek Symbols

α = M_B/M_A, molecular wieght ratio

η = z/L_0, dimensionless vertical coordinate

ρ = total mass density of liquid, Kg/m^3

τ = $D_{AB}t/L_0^2$, dimensionless time

τ_c = $Bi\ \tau$, dimensionless time

Literature Cited

Bird, R. B., W. E. Stewart and E. N. Lightfoot, Transport Phenomena, John Wiley & Sons, New York (1960).

Bouwmeester, R. J. B. and P. L. G. Vlek, "Rate Control of Ammonia Volatilization from Rice Paddies", Atmos. Environ., 15, 131-140 (1981).

Bouwmeester, R. J. B. and P. L. G. Vlek, "Wind Tunnel Simulation and Assessment of Ammonia Volatilization from Ponded Water", Agronomy J., 73, 546-552 (1981).

Briggs, G. A., "Plume Rise Predictions", Chapt. 3 in Lectures on Air Pollution and Environmental Impact, D. A. Haugen, editor, Am. Meteorol. Soc., Boston, MA (1975).

Britter, R. E., "The Spread of a Negatively Buoyant Plume in a Calm Environment", Atmos. Environ., 13, 1241-1247 (1979).

Carnahan, B., H. Luther and J. Wilkes, Applied Numerical Methods, John Wiley & Sons, New York (1969).

Cologer, P. C., "The Evaporation of a Volatile Chemical from a Two Component Spill" M.S. Thesis, University of Maryland, College Park, MD (1986).

Crank, J., The Mathematics of Diffusion, 2nd Ed., Oxford University Press, London (1975).

Davis, M. E., Numerical Methods and Modeling for Chemical Engineers, John Wiley & Sons, New York (1984).

Drivas, P. J., "Calculation of Evaporative Emissions for Multicomponent Liquid Spills", Environ. Sci. Technol., 16, 726-728 (1982).

Eidsvik, K. J., "Heavy Gas Dispersion Model with Liquified Release", Atmos. Environ., 15, 1163-1164 (1981).

Fay, J. A. and D. A. Ranck, "Comparison of Experiments on Dense Gas Cloud Dispersion", Atmos. Environ., 17, 239-248 (1983).

Fay, J. A. and S. G. Zemba, "Dispersion of Initially Compact Dense Gas Clouds", Atmos. Environ., 19, 1257-1261 (1985).

Feigley, C. E., "Comment on Calculation of Evaporative Emissions from Multicomponent Liquid Spills", Environ. Sci. Technol., 17, 311-312 (1983).

Harrison, W., M. A. Winnik, P. T. Y. Kwong and D. Mackay, "Crude Oil Spills: Disappearance of Aromatic and Aliphatic Components from Sea-Surface Slicks", Environ. Sci. Technol., 9, 231-234 (1975).

Mackay, D. and R. S. Matsugu, "Evaporation Rates of Liquid Hydrocarbon Spills on Land and Water", Can. J. Chem. Eng., 51, 434-439 (1973).

Mackay, D. and A. T. K. Yeun, "Mass Transfer Coefficient Correlations for Volatilization of Organic Solutes from Water", Environ. Sci. Technol., 17, 211-217 (1983).

Moein, G. J., "Magnitude of the Chemical Spill Problem: A Regional Overview", Proceedings of the 1978 National Conference on Control of Hazardous Material Spills", Miami Beach, FL, April 11-13 (1978).

de Nevers, N., "Spread and Downslope Flow of Negatively Buoyant Clouds", Atmos. Environ., 18, 2023-2027 (1984).

Slattery, J. C., Momentum, Energy and Mass Transfer in Continua, McGraw-Hill, New York (1972).

Toor, H. L., "Reference Frames in Diffusion", AIChE J., 8, 561 (1962).

Figure Captions

Figure 1. Liquid phase concentration profiles at various f_A for $w_0 = 0.5$ and $\alpha = 1$.

Figure 2. Cumulative fraction of A evaporated as a function of w_0 and Bi at $\alpha = 1$.

Figure 3. Cumulative fraction of A evaporated as a function of w_0 and α. a) Bi = 10, b) Bi = 1000.

Figure 4. Cumulative fraction of A evaporated for various Bi at $w_0 = 0.3$. Comparison of results from the general and limiting case models. a) $\alpha = 1$, b) $\alpha = 100$.

Figure 5. Cumulative fraction of A evaporated for various Bi predicted by the infinite dilution models. Comparison of results from the two resistance and limiting case models.

Figure 6. Transition curves showing region of validity of convection limited and diffusion limited models.

Figure 7. Cumulative fraction of A evaporated for the diffusion limited regime. The curves of constant w_0 apply to all appropriate Bi and α.

Figure 8. Cumulative fraction of A evaporated for the convection limited regime as a function of w_0 and α. The dependency on Bi is contained within τ_c.

Figure 9. Surface mass flux versus time as a function of Bi and w_0 at $\alpha = 10$. a) Large Bi: A plus sign indicates diffusion limited behavior at that and higher Bi. b) Small Bi: A minus sign indicates convection limited behavior at that and lower Bi.

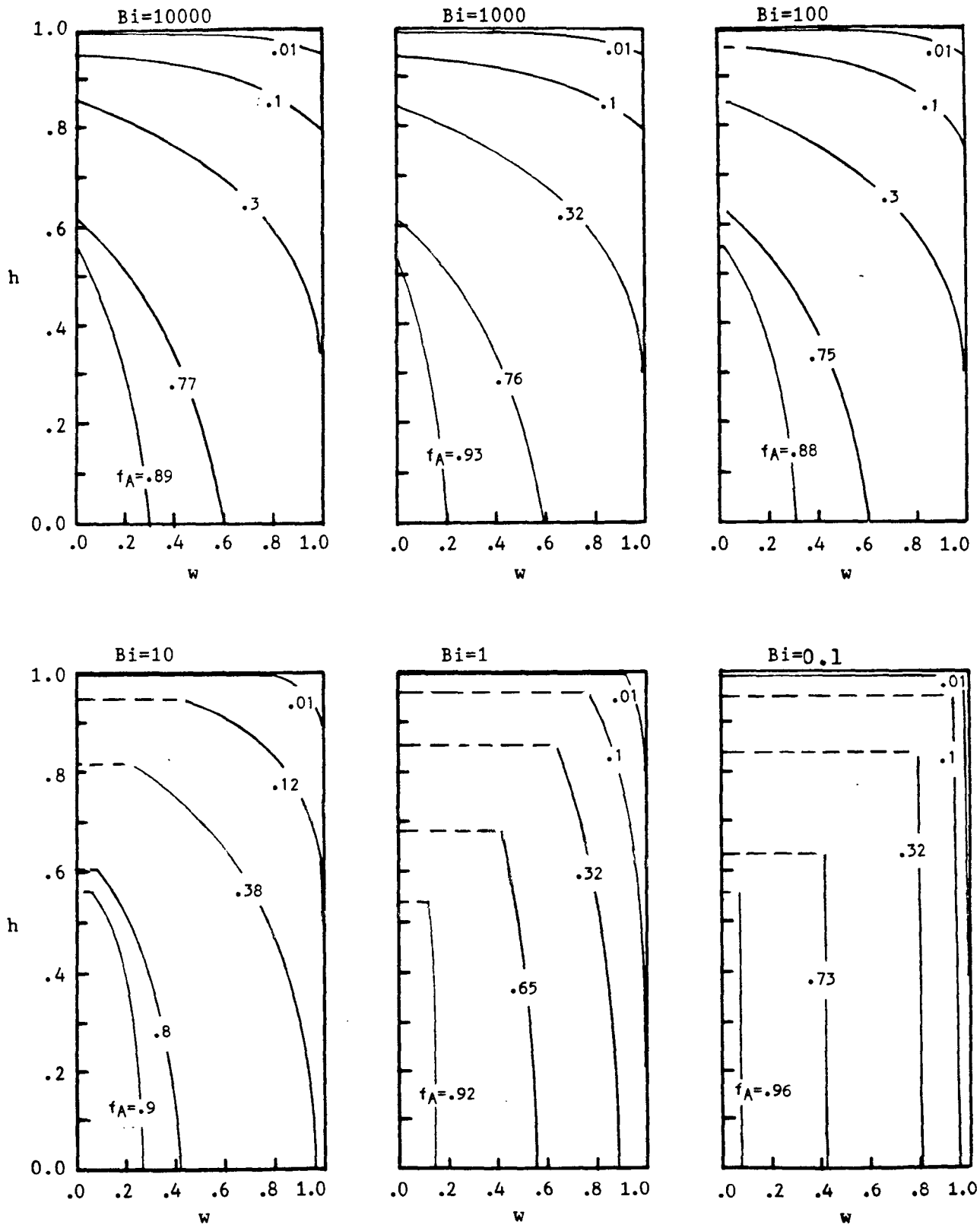
Bi=10000
Bi=1000
Bi=100
Bi=10
Bi=1
Bi=0.1
h
w
1.0
.8
.6
.4
.2
0.0
.0
.2
.4
.6
.8
1.0
.01
.1
.3
.32
.75
.77
.76
.12
.38
.8
.65
.73
f_A=.89
f_A=.93
f_A=.88
f_A=.9
f_A=.92
f_A=.96

Figure 1

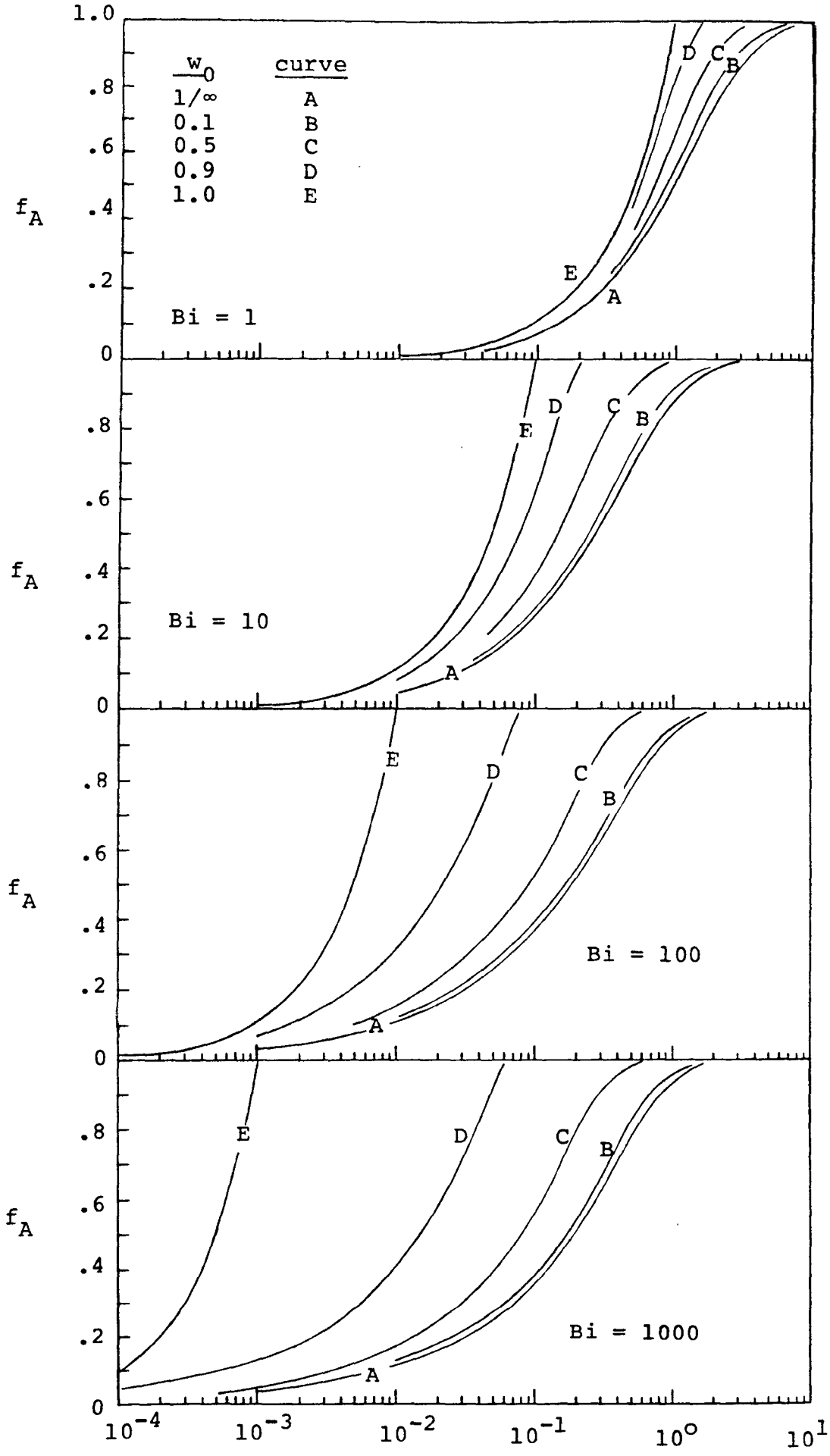
w_0 curve
1/∞ A
0.1 B
0.5 C
0.9 D
1.0 E
Bi = 1
Bi = 10
Bi = 100
Bi = 1000
f_A
1.0
.8
.6
.4
.2
0
A
B
C
D
E
10^{-4}
10^{-3}
10^{-2}
10^{-1}
10^{0}
10^{1}
τ

Figure 2

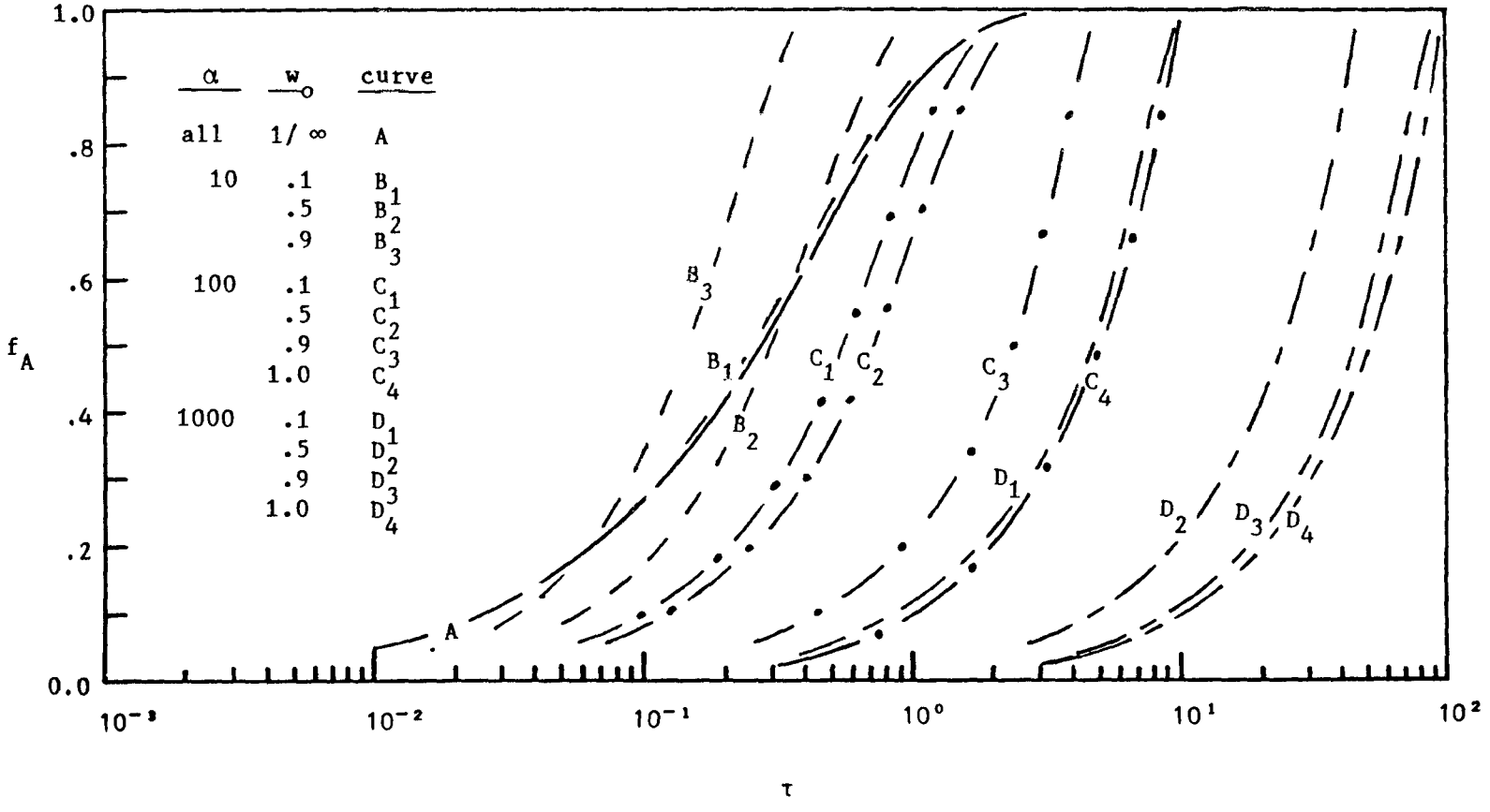
1.0
.8
.6
.4
.2
0.0
f_A
α
w_o
curve
all
1/ ∞
A
10
.1
B_1
.5
B_2
.9
B_3
100
.1
C_1
.5
C_2
.9
C_3
1.0
C_4
1000
.1
D_1
.5
D_2
.9
D_3
1.0
D_4
10^{-3}
10^{-2}
10^{-1}
10^{0}
10^{1}
10^{2}
τ

Figure 3a

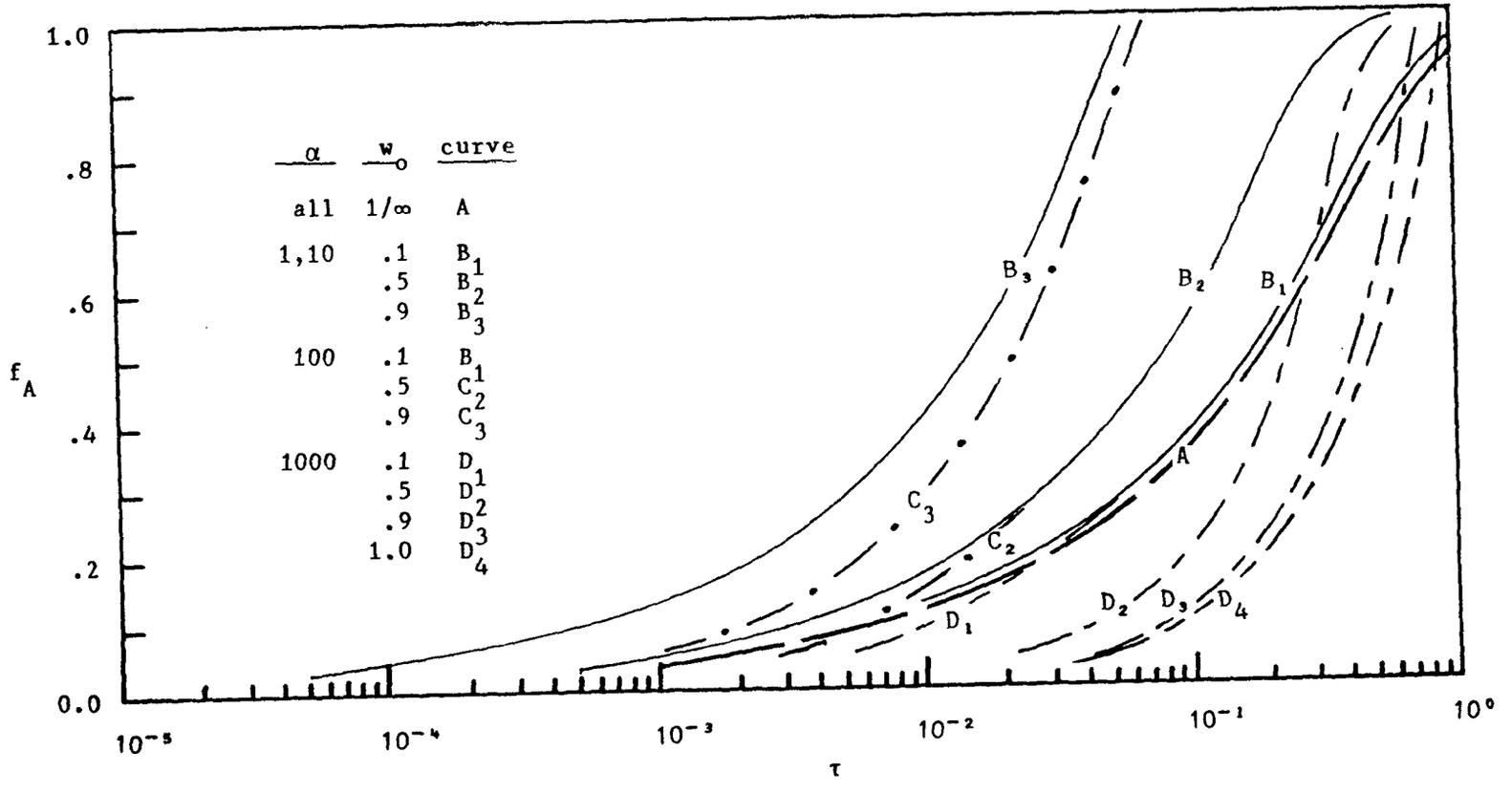
1.0
.8
.6
.4
.2
0.0
f_A
α
w_o
curve
all 1/∞ A
1,10 .1 B_1
.5 B_2
.9 B_3
100 .1 B
.5 C_2^1
.9 C_3^2
1000 .1 D
.5 D^1
.9 D^2
1.0 D_4^3
B_3
B_2
B_1
C_3
C_2
A
D_1
D_2
D_3
D_4
10^{-5}
10^{-4}
10^{-3}
10^{-2}
10^{-1}
10^{0}
τ

Figure 3b

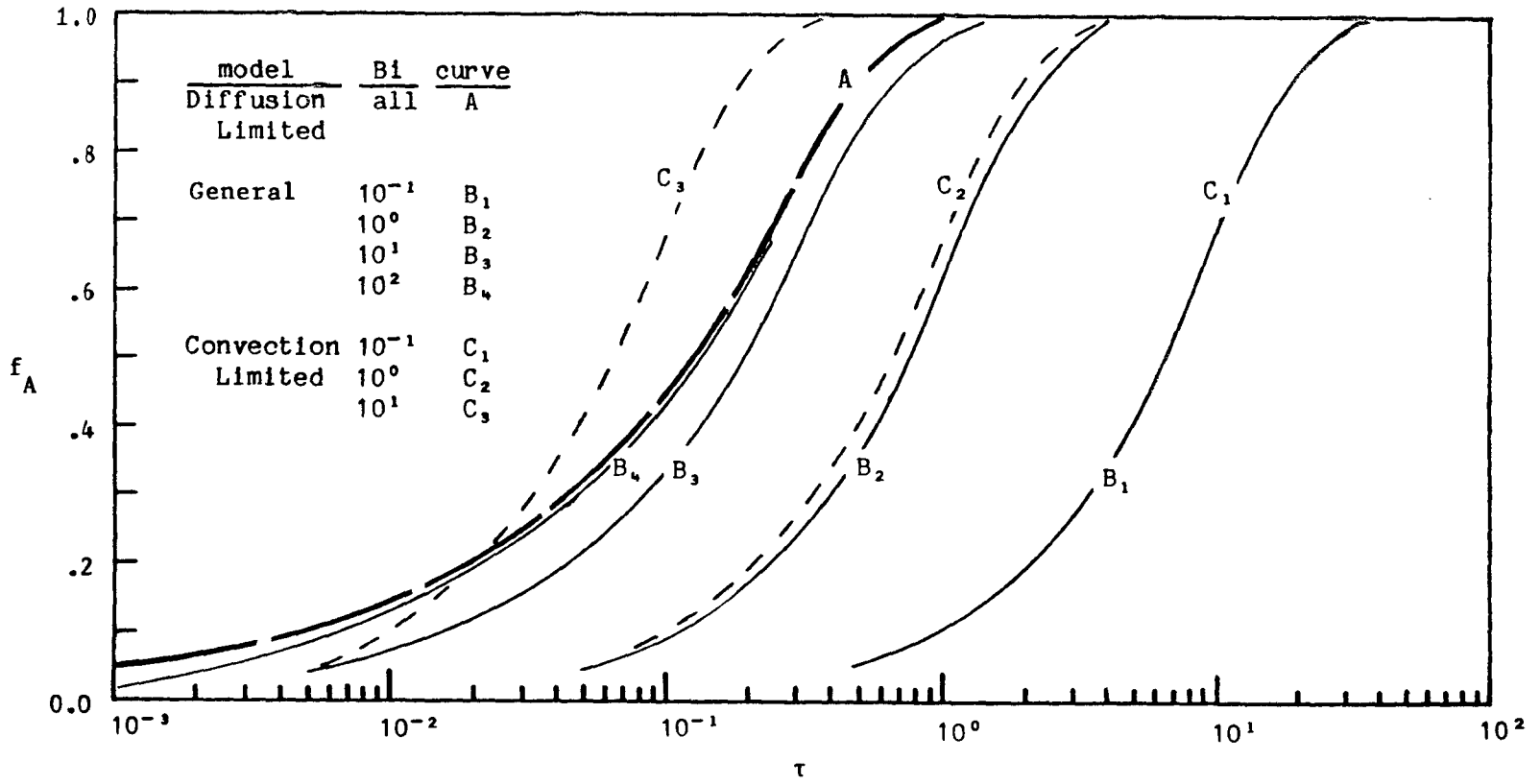
1.0
.8
.6
.4
.2
0.0
f_A
model
Bi
curve
Diffusion Limited
all
A
General
10^{-1}
B_1
10^{0}
B_2
10^{1}
B_3
10^{2}
B_4
Convection Limited
10^{-1}
C_1
10^{0}
C_2
10^{1}
C_3
A
C_3
C_2
C_1
B_4
B_3
B_2
B_1
10^{-3}
10^{-2}
10^{-1}
10^{0}
10^{1}
10^{2}
τ

Figure 4a

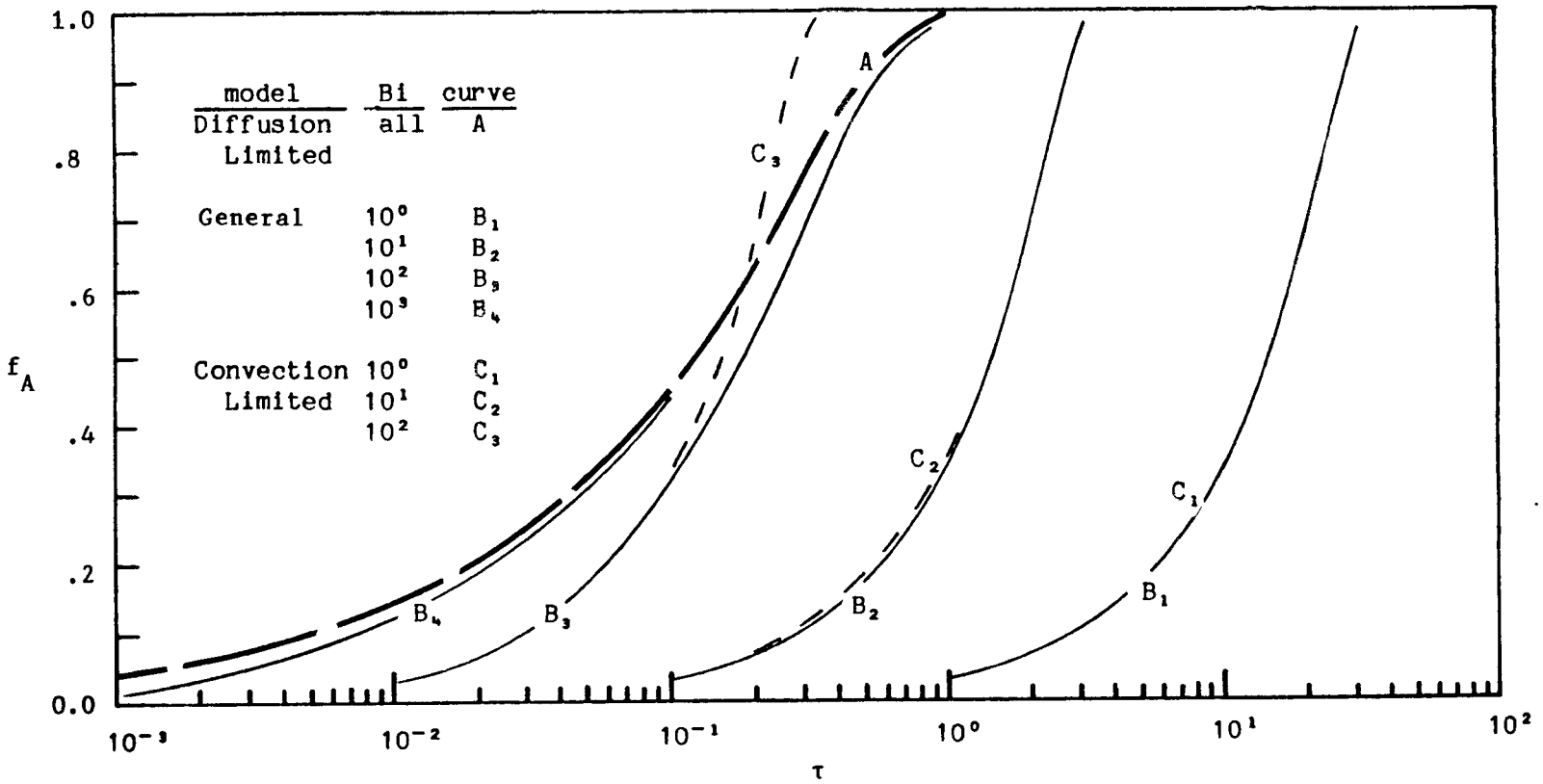
1.0
.8
.6
.4
.2
0.0
f_A
model
Bi
curve
Diffusion Limited
all
A
General
10^0
B_1
10^1
B_2
10^2
B_3
10^3
B_4
Convection Limited
10^0
C_1
10^1
C_2
10^2
C_3
A
C_3
C_2
C_1
B_4
B_3
B_2
B_1
10^{-3}
10^{-2}
10^{-1}
10^0
10^1
10^2
τ

Figure 4b

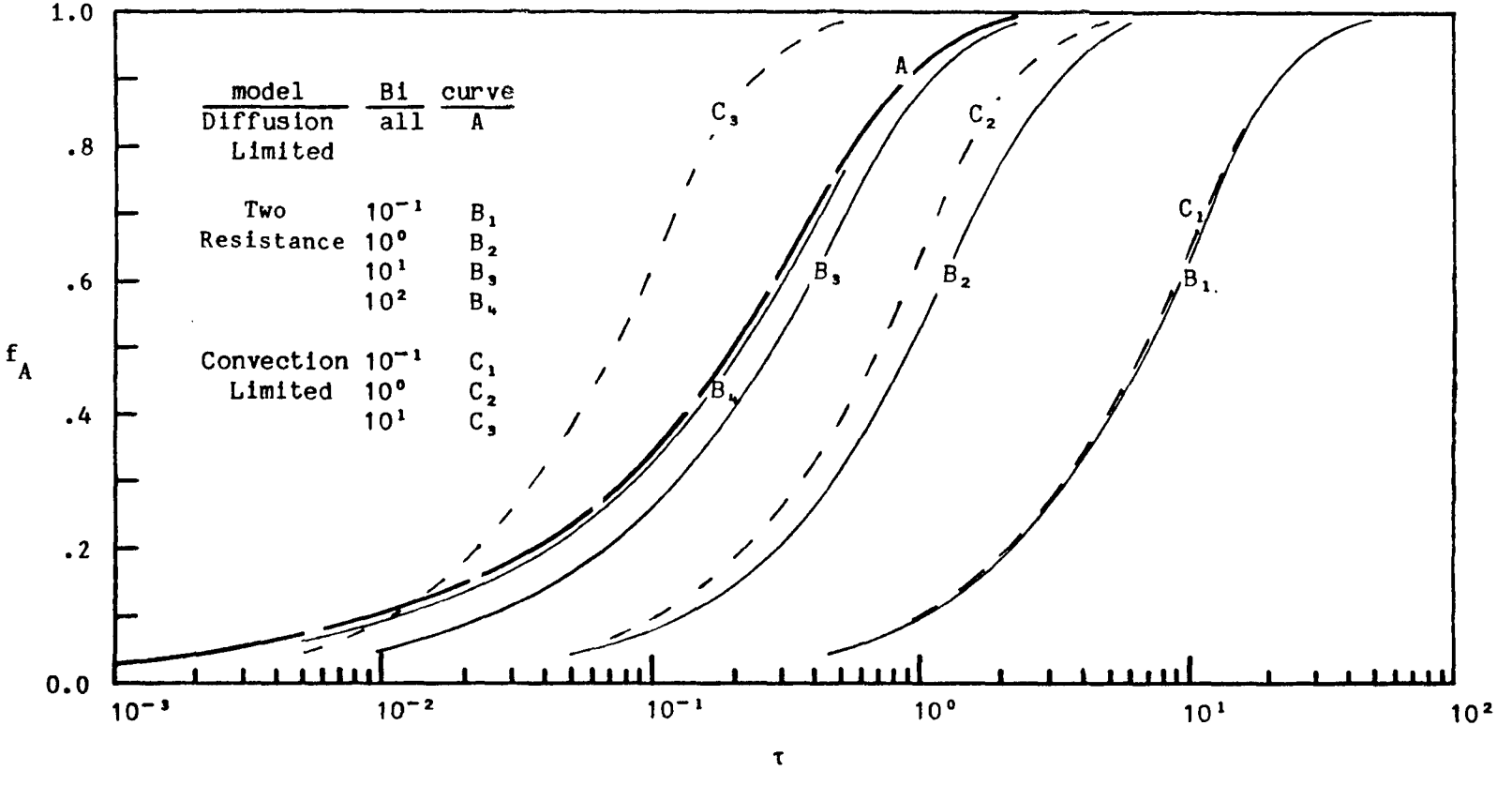
1.0
.8
.6
.4
.2
0.0
f_A
model
Bi
curve
Diffusion Limited
all
A
Two Resistance
10^{-1}
B_1
10^{0}
B_2
10^{1}
B_3
10^{2}
B_4
Convection Limited
10^{-1}
C_1
10^{0}
C_2
10^{1}
C_3
10^{-3}
10^{-2}
10^{-1}
10^{0}
10^{1}
10^{2}
τ

Figure 5

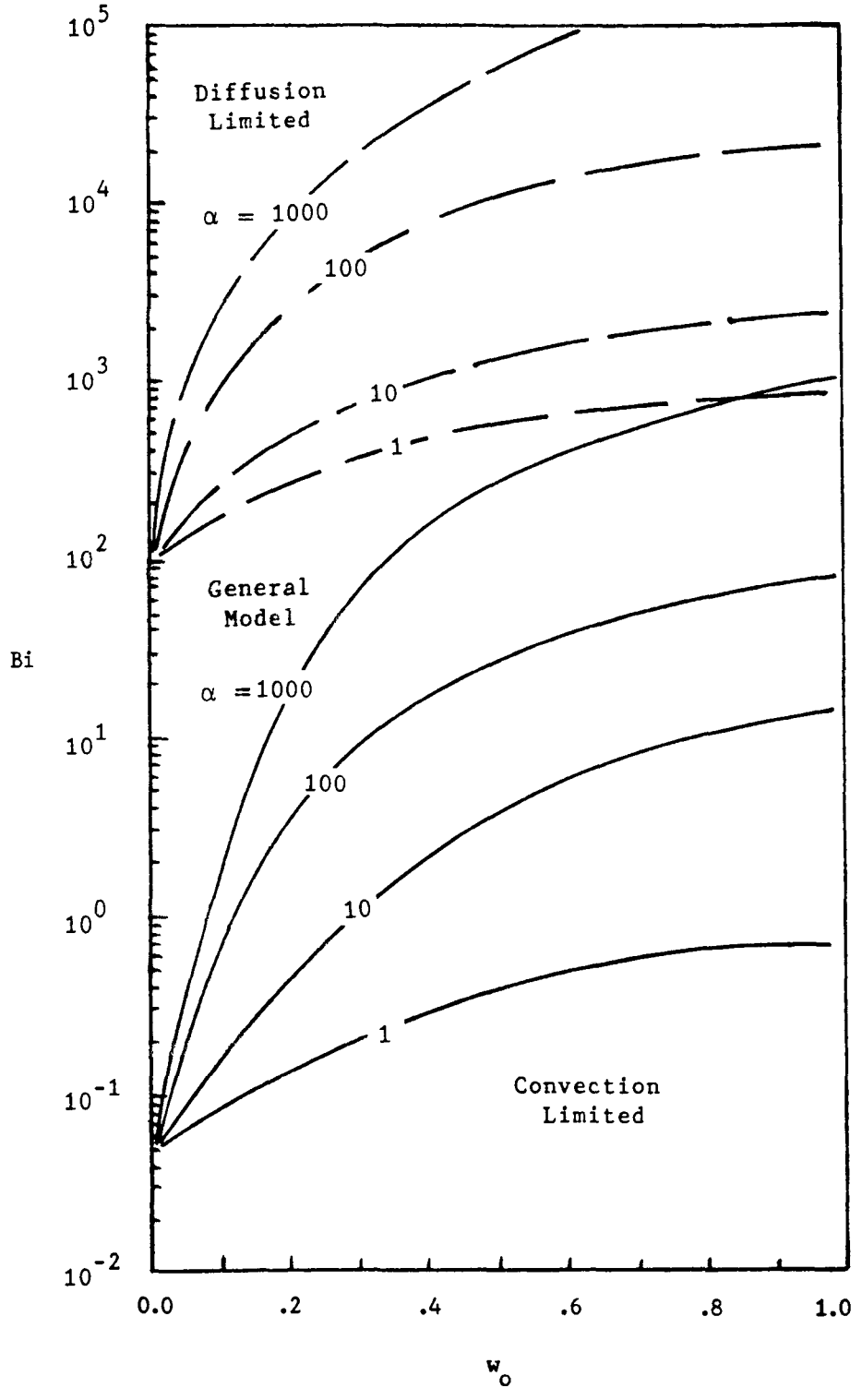
Diffusion Limited
α = 1000
100
10
1
General Model
α =1000
100
10
1
Convection Limited
Bi
10^5
10^4
10^3
10^2
10^1
10^0
10^{-1}
10^{-2}
0.0
.2
.4
.6
.8
1.0
w_o

Figure 6

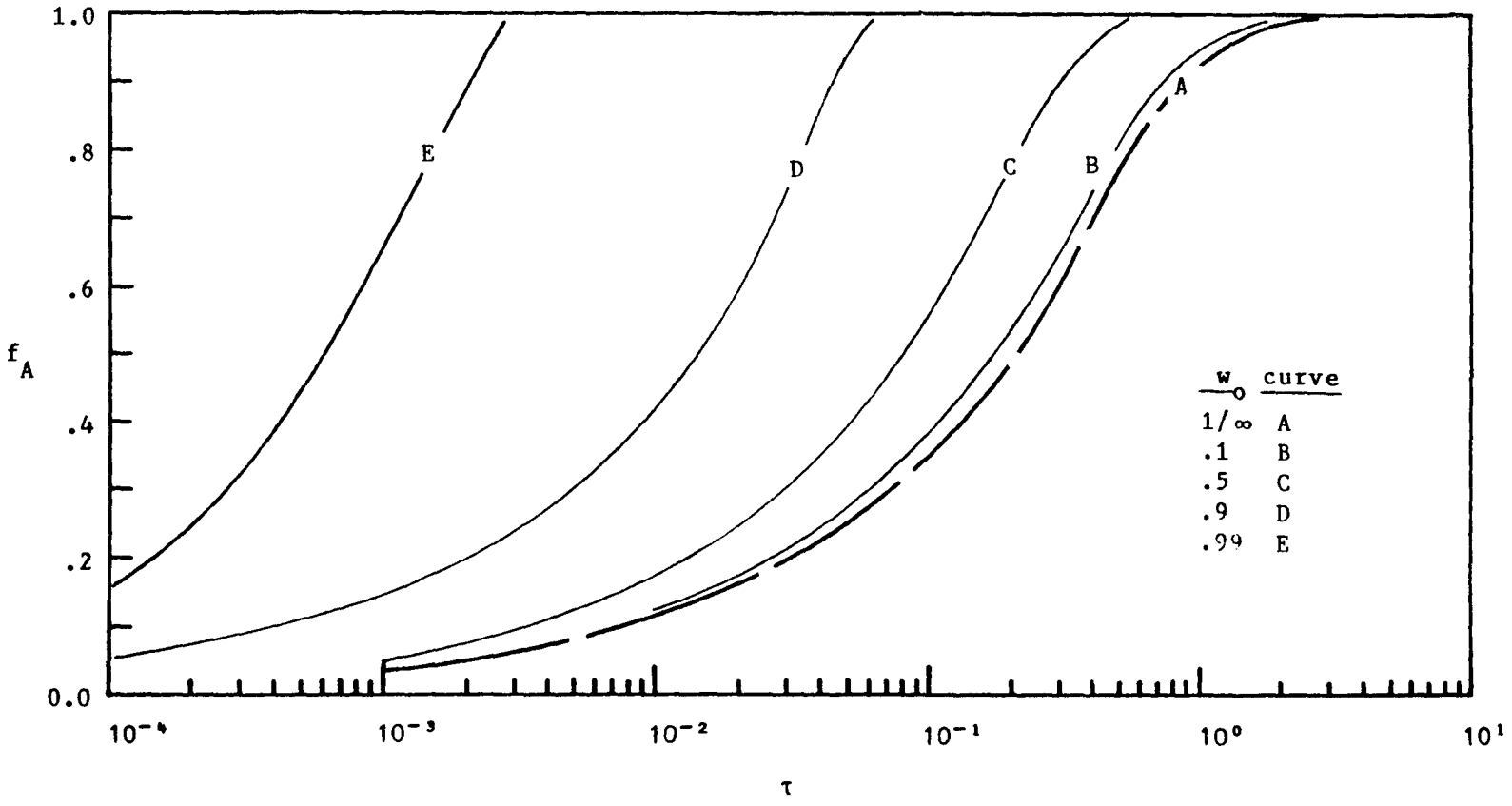
1.0
.8
.6
.4
.2
0.0
f_A
E
D
C
B
A
w_o curve
1/∞ A
.1 B
.5 C
.9 D
.99 E
10^{-4}
10^{-3}
10^{-2}
10^{-1}
10^{0}
10^{1}
τ

Figure 7

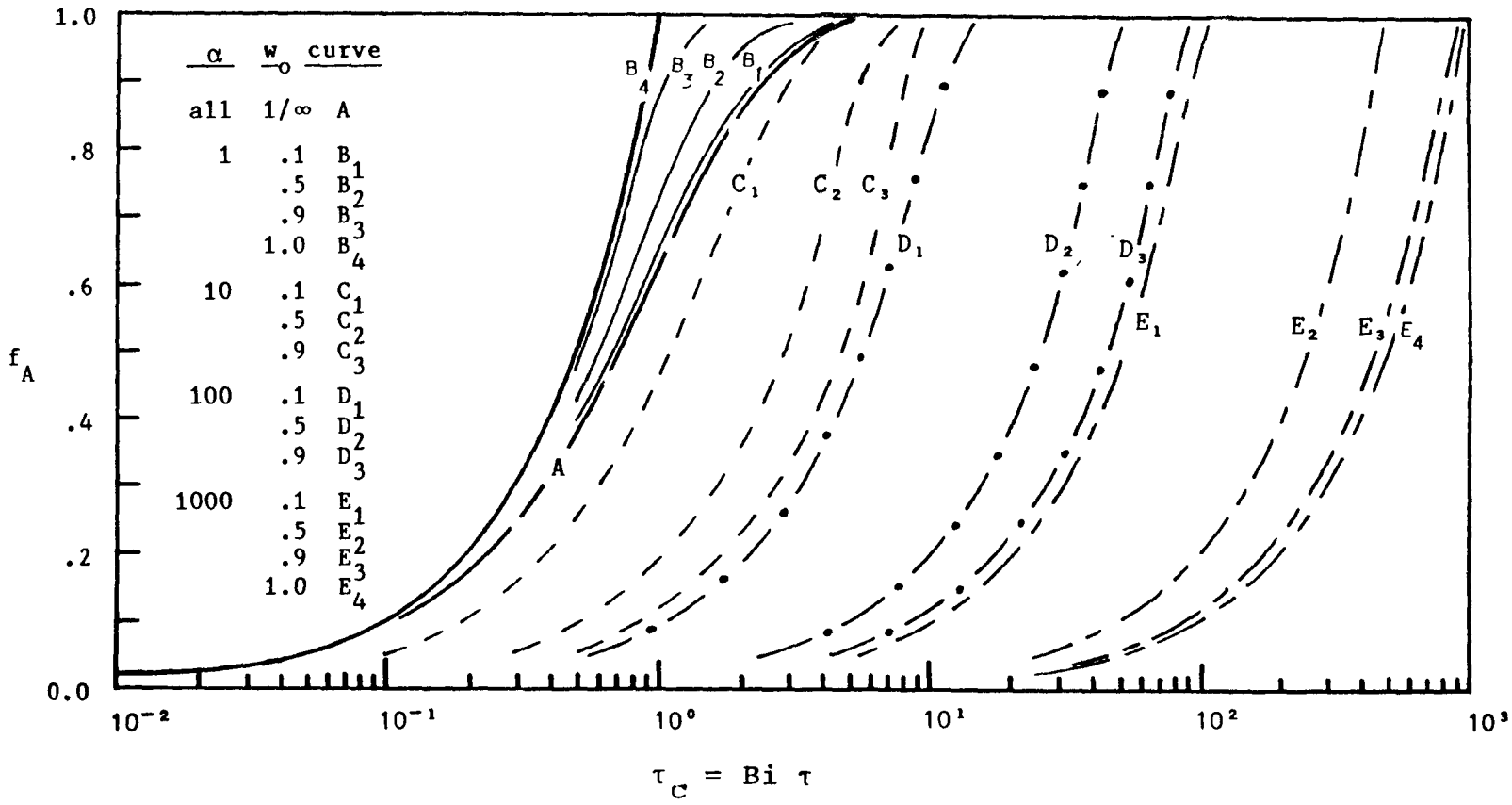
1.0
.8
.6
.4
.2
0.0
f_A
α
w_o
curve
all 1/∞ A
1 .1 B_1
.5 B_2
.9 B_3
1.0 B_4
10 .1 C_1
.5 C_2
.9 C_3
100 .1 D_1
.5 D_2
.9 D_3
1000 .1 E_1
.5 E_2
.9 E_3
1.0 E_4
10^{-2}
10^{-1}
10^{0}
10^{1}
10^{2}
10^{3}
τ_c = Bi τ

Figure 8

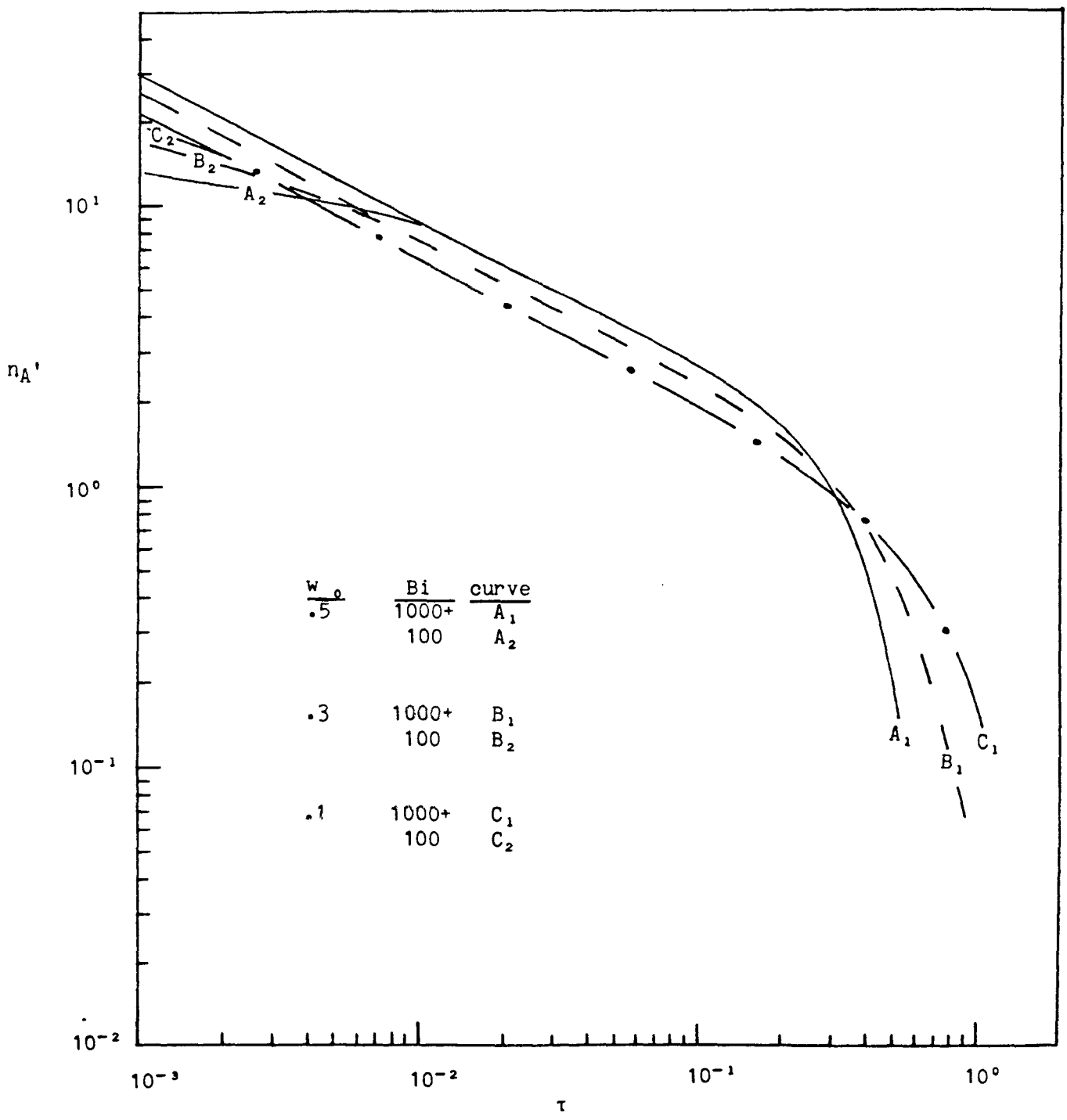
$n_{A'}$
10^{1}
10^{0}
10^{-1}
10^{-2}
10^{-3}
10^{-2}
10^{-1}
10^{0}
τ
C_2
B_2
A_2
A_1
B_1
C_1
w_o | Bi | curve
.5 | 1000+ | A_1
100 | A_2
.3 | 1000+ | B_1
100 | B_2
.1 | 1000+ | C_1
100 | C_2

Figure 9a

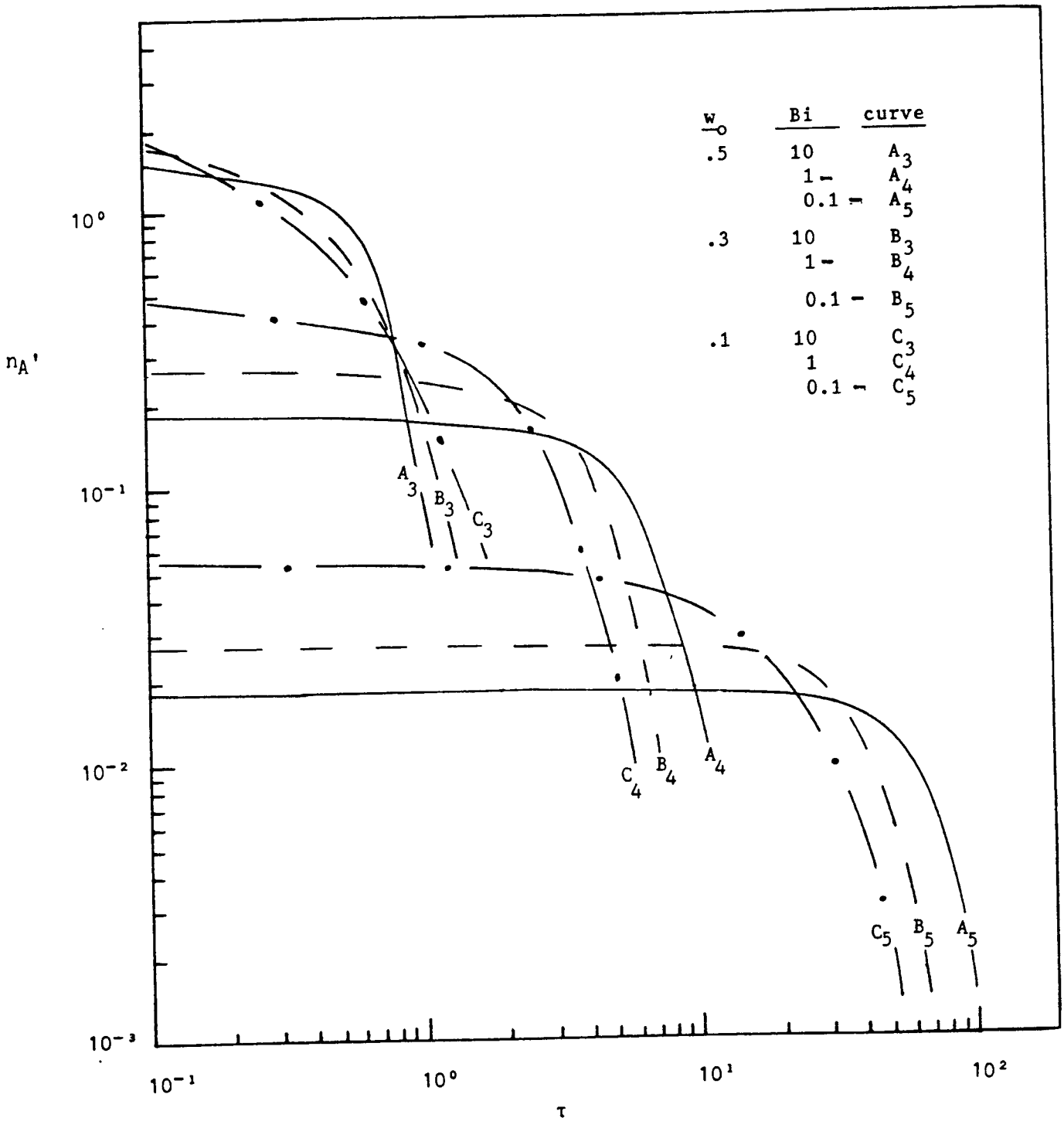
w_o Bi curve
.5 10 A_3
1 A_4
0.1 A_5
.3 10 B_3
1 B_4
0.1 B_5
.1 10 C_3
1 C_4
0.1 C_5
n_A'
10^0
10^{-1}
10^{-2}
10^{-3}
10^{-1}
10^0
10^1
10^2
τ

Figure 9b